PHYSICAL REVIEW B **90**, 180405(R) (2014)

Particle moment canting in $CoFe_2O_4$ nanoparticles

K. Hasz and Y. Ijiri*
Oberlin College, Department of Physics and Astronomy, Oberlin, Ohio 44074, USA

K. L. Krycka and J. A. Borchers
National Institute of Standards and Technology, NIST Center for Neutron Research, Gaithersburg, Maryland 20899, USA

R. A. Booth, S. Oberdick, and S. A. Majetich
Carnegie Mellon University, Department of Physics, Pittsburgh, Pennsylvania 15213, USA

(Received 10 September 2014; revised manuscript received 3 November 2014; published 19 November 2014)

Polarization-analyzed small-angle neutron scattering methods are used to determine the spin morphology in high crystalline anisotropy, 11 nm diameter $CoFe_2O_4$ nanoparticle assemblies with randomly oriented easy axes. In moderate to high magnetic fields, the nanoparticles adopt a uniformly canted structure, rather than forming domains, shells, or other arrangements. The observed canting angles agree quantitatively with those predicted from an energy model dominated by Zeeman and anisotropy competition, with implications for the technological use of such nanoparticles.

DOI: 10.1103/PhysRevB.90.180405 PACS number(s): 75.25.−j, 75.75.−c

Magnetic oxide nanoparticles are of interest in many applications ranging from ferrofluids to ultradense data storage to medical imaging and cancer therapy [1–3]. Particular attention has been paid to cobalt ferrite ($CoFe_2O_4$) nanoparticles [4,5], due to the high bulk anisotropy constant and reasonably large magnetization values [6–8]. While the success of these applications depends critically on the magnetic behavior, there are often deviations from bulk properties due to effects such as surface spin disorder [9], surface anisotropy [10], and exchange biasing [11].

Direct experimental determination of the underlying nanoparticle spin structure is very difficult, since typical macroscopic measurements average out the magnetization from distorted surface spins with little spatial sensitivity. Recently, electron microscopy methods have been used to probe individual iron oxide nanoparticles, revealing sensitive magnetization dependence to local surfactant bonding conditions [12]. However, these techniques typically investigate the nanoparticle structure in isolation as opposed to in more concentrated, potentially interacting conditions of interest for many applications.

Alternatively, using the recently developed technique of polarization-analyzed small-angle neutron scattering (PASANS) [13–15], we have been able to analyze the three-dimensional spatial distribution of magnetic moments in dense assemblies of iron oxide nanoparticles [16–18]. In that system, a magnetic core-shell morphology was observed [16], consistent with a model based on the careful energy minimization of exchange, interparticle dipolar coupling, Zeeman, and anisotropy energies [18].

Here, we test further the general applicability of this model by using PASANS methods on cobalt ferrite nanoparticles, where the anisotropy energy is an order of magnitude higher than for magnetite. In contrast to the aligned core and canted shell observed in iron oxide nanoparticles, we find for $CoFe_2O_4$ nanoparticles, uniformly rotated magnetic structures in high applied magnetic fields, consistent with a model dominated by the Zeeman and anisotropy energy contributions. While the overall magnetization within a particle is high as often desired for applications such as hyperthermia [3], the presence of a significant magnetic moment *not* along the field direction is a striking, unexpected feature that underscores the importance of direct measurement of nanoparticle spin structures.

The $CoFe_2O_4$ nanoparticles for this investigation were prepared by high temperature, nonaqueous solution chemistry methods as described previously, with oleic acid as the surfactant to prevent particle agglomeration [19]. Transmission electron microscopy (TEM) images, as illustrated in the inset to Fig. 1, were analyzed to determine a mean particle diameter of 11.0 nm ± 1.0 nm. Through a combination of alcohols with different evaporative rates [20], the nanoparticles were self-assembled into dense arrays with an apparent close-packed face centered cubic (fcc) stacking determined through microscopy images. A SQUID (superconducting quantum interference device) based magnetometer was used to measure magnetic moment versus applied magnetic field and temperature, as shown in Fig. 1, with bulk measurements obtained from polycrystalline powder of $CoFe_2O_4$ from Alfa Aesar [21]. The magnetometry data indicate the expected enhancement in the coercivity for nanoparticles over bulk material at low temperature, along with the decreasing coercivity as a function of increasing temperature in contrast to the bulk which had only minor coercivity temperature dependence. The dense arrays of nanoparticles were sealed in aluminum cells for neutron scattering measurements.

Polarization-analyzed SANS experiments were performed at the NIST Center for Neutron Research using the NG3 and NG7 SANS instruments, an in-beam FeSi supermirror polarizer to polarize the incident neutrons, a polarized ^{3}He cell in transmission geometry as a spin analyzer, a radio frequency (RF) or aluminum coil spin flipper for the incident neutrons, and an *in situ* NMR flipper for the scattered neutrons [14].

*yumi.ijiri@oberlin.edu

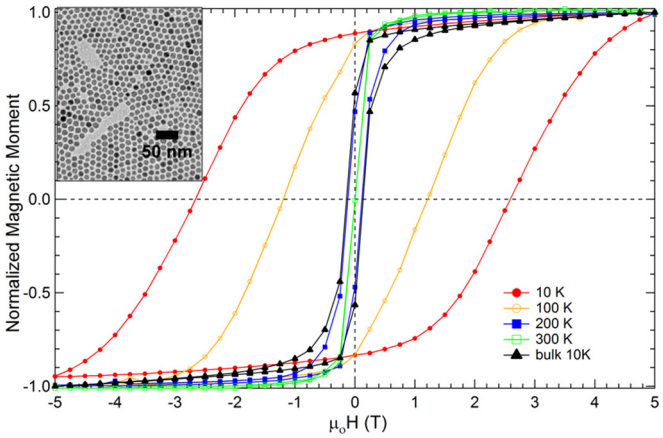

FIG. 1. (Color online) Hysteresis loops for $CoFe_2O_4$ nanoparticle assemblies at 10, 100, 200, and 300 K. The 10 K hysteresis loop for bulk $CoFe_2O_4$ is shown for comparison. Inset shows TEM image of as-grown particles.

The sample was cooled in a closed-cycle He refrigerator, and an electromagnet was used to apply magnetic fields ($\mu_o H$) at 1.4 T, the maximum attainable value. Data were collected in transmission with a two-dimensional (2D) detector at two different distances to span the scattering vector $\vec{Q}$ range from $\approx$0.01 Å^{-1} to 0.15 Å^{-1}. Figure 2(a) illustrates the setup with the neutron beam along Z, the applied field along X, the detector in the X-Y plane, and the angle ϕ between $\vec{Q}$ and X. Corrections for the time-dependent decay of the ^{3}He polarization, inefficiencies in the supermirror and flippers, and detector inhomogeneities were made, and the data were reduced as described previously [14,22]. With the neutron polarization state denoted as + or −, applying these corrections then yielded the measurement of all four neutron spin cross sections (+ +, − −, − +, and + −) corresponding to either initially + or − spin state neutrons scattering into + or −

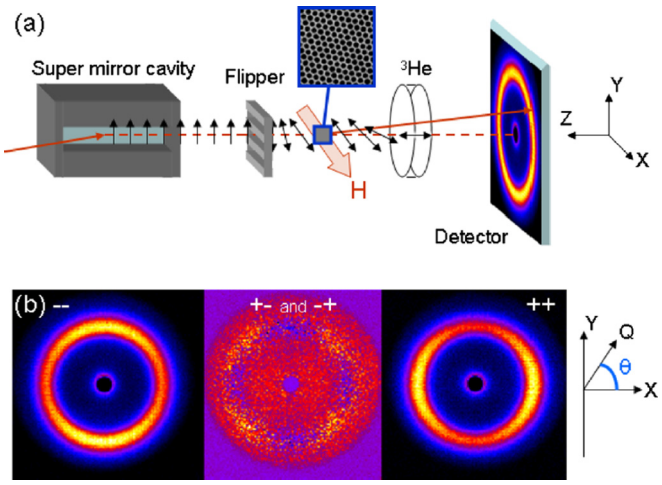

FIG. 2. (Color online) (a) Experimental setup includes a polarizing supermirror and RF or conventional flipper to select the incident spin state and a ^{3}He cell with *in situ* NMR flipper to select the scattered spin state. The scattering pattern is collected on a 2D detector. (b) Corrected 2D SANS images for 200 K, 1.4 T.

neutrons. Examples of the corrected 2D SANS images are shown in Fig. 2(b).

The measured scattering intensity I is proportional to combinations of the nuclear and magnetic structure of the sample. Since the sample is macroscopic with a thickness of $\approx$1 mm, it is assumed to be structurally isotropic with only the applied field direction X unique. With these assumptions for our beam geometry and special ϕ angles of either 0° or 90°, the spin selection rules simplify to [17]

$$I^{++,--}_{\phi=0^\circ} = N^2, \tag{1}$$

$$I^{++,--}_{\phi=90^\circ} = N^2 + M_X^2 \mp 2NM_X, \tag{2}$$

$$I^{+-,-+}_{\phi=0^\circ} = M_Y^2 + M_Z^2 = 2M^2_{\mathrm{PERP}}, \tag{3}$$

$$I^{+-,-+}_{\phi=90^\circ} = M_Z^2 = M^2_{\mathrm{PERP}}, \tag{4}$$

where N, M_X, M_Y, and M_Z are the spatial Fourier transforms of the structural and magnetic scattering. Since only the field direction X is unique, we can define $M_X^2 = M^2_{\mathrm{PARL}}$ as the square of the parallel to the field magnetic Fourier transform and $M_Y^2 = M_Z^2 = M^2_{\mathrm{PERP}}$ as the square of the perpendicular to the field magnetic Fourier transform.

Application of these expressions yields consistent structural (N^2) data for a variety of temperature and field conditions as illustrated in Fig. 3(a). The data display a characteristic Bragg peak, indicating that the structural order persists over multiple nanoparticles; the sample is modeled well by a fcc lattice of nanoparticles with diameter 10 nm ± 1 nm and

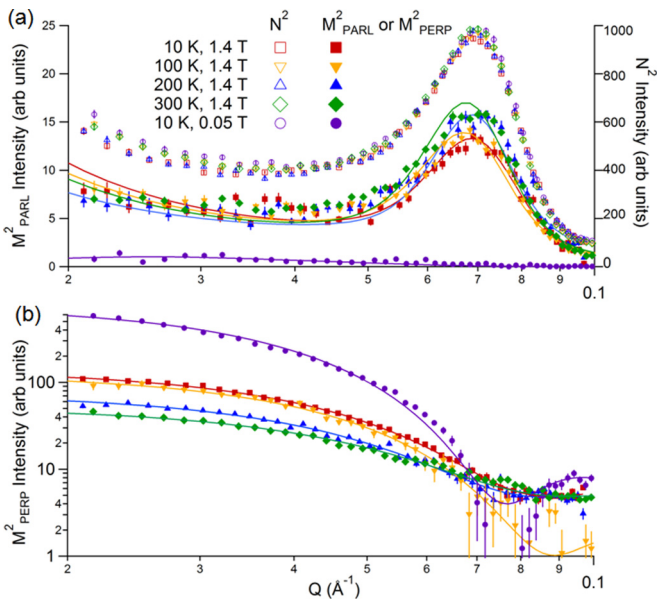

FIG. 3. (Color online) (a) Data for N^2 and M^2_{PARL} vs Q and (b) M^2_{PERP} vs Q for a variety of temperatures in 1.4 T, scaled to a N^2 Bragg peak height of 1000. Data for 10 K in a remanent field of $\approx$0.05 T are also shown. Solid lines in (a) are for a close-packed array of fcc magnetic spheres with $\approx$13% standard deviation in spacing distance whereas for (b) are for simple spheres of diameter 10.5 nm ± 0.4 nm. Error bars in the plot denote standard uncertainties.

lattice spacing of 15 nm ± 1 nm, consistent with the TEM results. The characteristic magnetic signature along the field direction, M^2_{PARL}, is much weaker but mimics the shape of the structural scattering in high field, indicating coherence over multiple nanoparticles. It is most intense at high temperature and high field; a significantly smaller, almost negligible signal is observed in the ≈0.05 T magnet remanent field.

In contrast to the field direction behavior, the M^2_{PERP} signal shows a pattern consistent with uncorrelated spheres [Fig. 3(b)], indicating that the perpendicular component of the magnetization is not aligned from one particle in the array to the next, as expected for particles with randomly oriented magnetocrystalline easy axes. As illustrated by the solid model lines, the magnetic signals fit to those expected for simple spheres of diameter 10.5 nm ± 0.4 nm, consistent with the TEM measured nanoparticle diameter. Thus, the data at different field and temperature conditions vary solely on the magnitude of the signal, with low field and low temperature producing the largest M^2_{PERP} signal.

Since both the M_{PERP} and M_{PARL} signals at high field are associated with spheres matching the measured nanoparticle sizes, we interpret the observed PASANS behavior in terms of magnetic particles of uniform net magnetization throughout but canted in an applied field, in contrast to the situation for iron oxide nanoparticles which exhibited a core and a shell of different sizes and net moment orientations [16]. For these $CoFe_2O_4$ nanoparticles, the parallel to field component is coherent over multiple nanoparticles, while the perpendicular component persists only over a single particle, as a result of there being multiple ways to cant. Recognizing then that the observed M_{PERP} and M_{PARL} Fourier transforms should be proportional to the underlying related magnetic moments m_{PERP} and m_{PARL} and accounting for the contributions to M_{PERP} in both Y and Z, we can define a magnetic particle canting angle θ

$$\theta \equiv \tan^{-1}\left(\frac{m_{PERP}}{m_{PARL}}\right) = \tan^{-1}\left(\sqrt{\frac{2M^2_{PERP}}{M^2_{PARL}}}\right). \quad (5)$$

With this definition and the data in Fig. 3, we find a particle canting angle in high field that decreases from 33° to 17° as the temperature is increased from 10 K to 300 K, as listed in Table I. Some moment canting can be expected for the 10 K and 100 K data in 1.4 T, which from Fig. 1 should correspond to conditions away from saturation. Here, the small particle size makes coherent canting of the spins within a single nanoparticle a plausible spin structure vs the more complicated picture expected for bulk cobalt ferrite, involving domains and domain walls.

TABLE I. Intensity of M^2_{PERP}, M^2_{PARL} (scaled against structural N^2 set to 1000), and measured and modeled canting angles. Measured uncertainties are standard deviations. The comparatively larger uncertainties in the model stem in part from the flatness of the energy minima.

Condition	M^2_{PERP}	M^2_{PARL}	Measured θ	Modeled θ
10 K, 1.4 T	2.9 ± 0.2	13.5 ± 0.5	33° ± 2°	33° ± 4°
100 K, 1.4 T	2.8 ± 0.2	14.2 ± 0.5	32° ± 2°	32° ± 4°
200 K, 1.4 T	1.5 ± 0.2	15.8 ± 0.5	24° ± 2°	26° ± 4°
300 K, 1.4 T	0.86 ± 0.07	17.1 ± 0.5	17° ± 2°	17° ± 4°

However, note that the PASANS data indicate sizable canting is also observed at 200 K and 300 K in 1.4 T, which are very near saturation. The presence of large canting values in these cases provides an explanation for the commonly observed phenomena that the measured SQUID saturation magnetization for nanoparticles is often reduced from bulk, here with a room temperature saturation value of 62 ± 7 A m^2/kg (emu/g) vs the ≈76 emu/g for bulk $CoFe_2O_4$ [6–8] [23]. Note this is in contrast to other explanations often used to understand saturation reduction in terms of either surface spin disorder or a shell of spins of another orientation as was seen for Fe_3O_4 [16]. Another common explanation, a reduced magnetization or surface "dead layer," is less likely to apply in this case, given that for related Fe_3O_4 nanoparticles with oleic acid, the surfactant was found to help maintain the surface magnetization [12].

To test more quantitatively the physical significance of the observed canting angles and to understand the origins, we have modeled the nanoparticle system by considering each ≈11 nm diameter nanoparticle to be made of a set of small cubes of side length 0.42 nm, corresponding to one formula unit (f.u.) of $CoFe_2O_4$. As we have no direct evidence of site occupancy deviations from bulk $CoFe_2O_4$, the formula unit cubes are assumed to have inverse spinel structure with three interstitial sites filled with magnetic ions. From the standard model for these ferrites, the tetrahedral site is expected to be filled with an Fe magnetic moment of 5 μ_B and the two octahedral sites are to be occupied with magnetic moments for Co of 3 μ_B and for Fe of 5 μ_B as illustrated in Fig. 4(a). Generalizing, we let the individual sites cant in an applied magnetic field **H** to change the magnetic moment of the formula unit, resulting in

$$m_{PARL} \propto 8\,\mu_B \cos(O_h) - 5\,\mu_B \cos(T_d), \quad (6)$$

$$m_{PERP} \propto 8\,\mu_B \sin(O_h) - 5\,\mu_B \sin(T_d), \quad (7)$$

where O_h is the averaged tilt angle of the octahedral site and T_d is the tilt angle of the tetrahedral site. In bulk $CoFe_2O_4$ with no applied magnetic field, the tetrahedral site is usually aligned nearly antiparallel to the octahedral sites via exchange interactions to give a net magnetization of 3.94 μ_B per formula unit at 0 K and ≈3.3 μ_B at 300 K, due to thermal excitations [7,8]. Note that based on bulk behavior, strong site coupling should cause the moments to cant together within a single particle, yielding $O_h = T_d = \theta$, as shown in Fig. 4(a). The 11 nm nanoparticle spheres are then modeled as a closed packed assembly with lattice spacing of 15 nm.

In previous work modeling the energetics of iron oxide nanoparticles [18], the contributions of Zeeman and exchange energy dominated, with magnetocrystalline anisotropy and inter-nanoparticle dipolar energy adding important contribution to shape the local energy minima with respect to different spin structures, resulting in canted shells and aligned cores in high magnetic fields.

Here, we have investigated these contributions for $CoFe_2O_4$ nanoparticles modeled as described above. The expected anisotropy constant is much larger (over an order of magnitude and of opposite sign to the $K = -13$ kJ/m^3 for Fe_3O_4 at

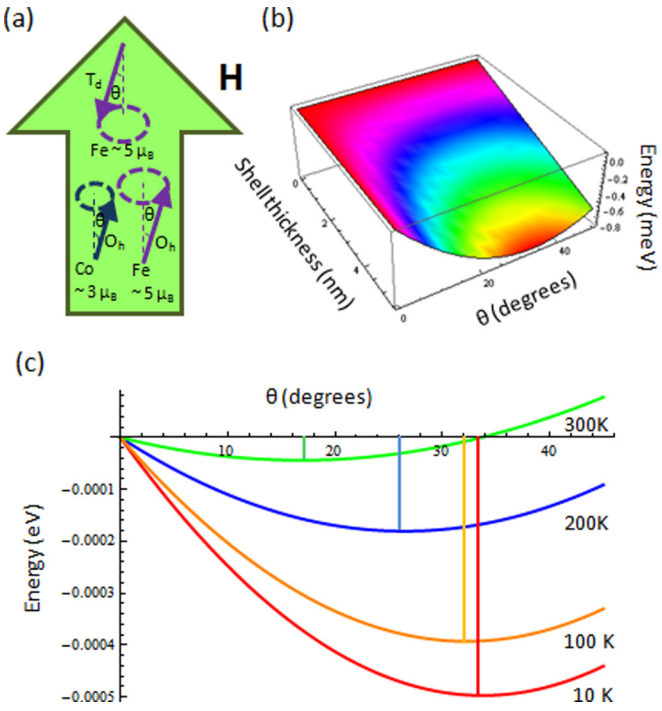

FIG. 4. (Color online) (a) Modeling $CoFe_2O_4$ with tilted angles for T_d and O_h sites referenced relative to an applied field **H** (green arrow). Angles are shown for the case of $O_h = T_d = \theta$; possible thermal excitations are indicated by dotted circular orbits. (b) Energy landscape for 10 K, 1.4 T showing minimum energy for no shell formation. (c) Energy savings per formula unit from canting in 1.4 T at 10 K (red), 100 K (orange), 200 K (blue), and 300 K (green). Minima are denoted by vertical lines.

room temperature), so that a simpler model with only Zeeman energy and anisotropy can capture the essential physics. For $CoFe_2O_4$, the energy savings caused by canting toward the randomly oriented easy axes are greater than the Zeeman cost of canting away from the applied magnetic field. The dipole and exchange terms are insufficient to support the formation of a core and shell structure as in the case for Fe_3O_4. Since the net M_{PARL} signal from nanoparticle to nanoparticle is long-range as shown in Fig. 3(a), the overall minimized energy structure can be described by a single canting angle for the nanoparticle structure as shown in Fig. 4(a) and simulated in Fig. 4(b).

In more detail, we have included the anisotropy constant temperature dependence using the phenomenological expression found for bulk ($K = 1.96 \times 10^6 e^{-1.90\times10^{-5}T^2}$ J/m^3), along with the bulk temperature dependent magnetic moment per formula unit (which varies from 3.94 μ_B at 0 K to 3.3 μ_B at 300 K) [7] such that the key terms controlling the energy per formula unit are

$$E_{\text{f.u.}} = mH[1 - \cos(\theta)] - K[\cos(45^\circ - \theta) - \cos(45^\circ)], \quad (8)$$

where m is the moment of the particle (scaled with temperature), H is the magnitude of the applied magnetic field, θ is the canting angle, K is the anisotropy constant per formula unit, and 45° is the maximum angle between H and the nearest (100) anisotropy axis.

As shown in Fig. 4(c) and listed in Table I, these energy terms lead to minima in the total energy per formula unit at different tilt angles for various temperature conditions in a high magnetic field. Note that the simulated angles of energy minima are in excellent agreement with those determined from the PASANS data.

To test the robustness of this modeling, we have investigated several assumptions for the energetics of the $CoFe_2O_4$ nanoparticles. Instead of a single tilt of $O_h = T_d = \theta$, we also explored the possibility of tipping O_h and T_d independently, as was done for Fe_3O_4 [18]. This generalization did not produce any lower energy landscapes for the $CoFe_2O_4$ nanoparticle system. The model is also sensitive to the choice of easy axis. Unlike other ferrites with a preferred ⟨111⟩ set of directions, $CoFe_2O_4$ in bulk is observed to have preferred ⟨100⟩ axes due the difference in sign in the anisotropy constant. Using ⟨100⟩ easy axis directions and a uniform distribution of crystallite orientations were essential assumptions for the excellent model agreement with the PASANS data. Furthermore, changes of the anisotropy constant by more than 75% led to significant changes in the canting angle, thus placing some limits to the $CoFe_2O_4$ nanoparticle anisotropy [7].

Given the excellent agreement between model and experiment, we have also studied the energy landscapes at low temperature (10 K) as a function of applied magnetic field. We find that even in magnetic fields as high as 10 T, a noticeable 10° tilt is still expected, indicating the widespread prevalence of this canting configuration and the need to consider such an arrangement in many technological uses of these particles.

In conclusion, we have used advanced PASANS methods to directly determine the spin structure in $CoFe_2O_4$ nanoparticle assemblies. In high magnetic field, we find particle moment canting that decreases with increasing temperature. The observed canting angles agree with an energy model considering primarily the strong $CoFe_2O_4$ anisotropy against a Zeeman field term and help explain the lower SQUID magnetization compared to bulk $CoFe_2O_4$. Remarkably, when the canting is taken into account, the ratio of magnetization at 300 K vs 10 K is 99% ± 3% (Table I), a negligible thermal response as desired for many applications. Taken together with our earlier study on Fe_3O_4, these results provide further evidence of the range of possible magnetic nanoparticle spin structures and the utility of an energy balance model to understand them. These findings are particularly importance given the very common observation of non-bulk-behavior in magnetic nanoparticles and the need to interpret and tailor such behavior.

This work was partially supported by the National Science Foundation (NSF) DMR-1104489 and an Oberlin College Research Status Award. The research made use of facilities supported from NSF DMR-0944772. R.A.B., S.D.O., and S.A.M. acknowledge support by the DOE through Grant No. DEFG0208ER4648. We thank W. C. Chen and S. M. Watson for their assistance with the polarized ^{3}He spin filters.

[1] S. Odenbach, J. Phys. Condens. Matter **16**, R1135 (2004).
[2] Z. Z. Bandic and R. H. Victora, Proc. IEEE **96**, 1749 (2008).
[3] K. Krishnan, IEEE Trans. Magn. **46**, 2523 (2010).
[4] P. A. Kumar, S. Ray, S. Charkraverty, and D. D. Sarma, Appl. Phys. Lett. **103**, 102406 (2013).
[5] S. Amiri and H. Shokrollahi, Mater. Sci. Eng. C **33**, 1 (2013).
[6] R. Pauthenet, Ann. Phys.-Paris **7**, 710 (1952).
[7] H. Shenker, Phys. Rev. **107**, 1246 (1957).
[8] J. C. Slonczewski, J. Appl. Phys. **32**, S253 (1961).
[9] R. H. Kodama, A. E. Berkowitz, E. J. McNiff, and S. Foner, Phys. Rev. Lett. **77**, 394 (1996).
[10] D. A. Garanin and H. Kachkachi, Phys. Rev. Lett. **90**, 065504 (2003).
[11] V. Skumryev, S. Stoyanov, Y. Zhang, G. Hadjipanayis, D. Givord, and J. Nogués, Nature (London) **423**, 850 (2003).
[12] J. Salafranca, J. Gazquez, N. Pérez, A. Labarta, S. T. Pantelides, S. J. Pennycook, X. Batlle, and M. Varela, Nano Lett. **12**, 2499 (2012).
[13] R. M. Moon, T. Riste, and W. C. Koehler, Phys. Rev. **181**, 920 (1969).
[14] K. L. Krycka, R. Booth, J. A. Borchers, W. C. Chen, C. Conlon, T. R. Gentile, C. Hogg, Y. Ijiri, M. Laver, B. B. Maranville, S. A. Majetich, J. J. Rhyne, and S. M. Watson, Physica B **404**, 2561 (2009).
[15] D. Honecker, A. Ferdinand, F. Döbrich, C. D. Dewhurst, A. Wiedenmann, C. Gómez-Polo, K. Suzuki, and A. Michels, Eur. Phys. J. B **76**, 209 (2010).
[16] K. L. Krycka, R. A. Booth, C. R. Hogg, Y. Ijiri, J. A. Borchers, W. C. Chen, S. M. Watson, M. Laver, T. R. Gentile, L. R. Dedon, S. Harris, J. J. Rhyne, and S. A. Majetich, Phys. Rev. Lett. **104**, 207203 (2010).
[17] K. L. Krycka, J. Borchers, Y. Ijiri, R. A. Booth, and S. Majetich, J. Appl. Cryst. **45**, 554 (2012).
[18] K. L. Krycka, J. A. Borchers, R. A. Booth, S. A. Majetich, Y. Ijiri, K. Hasz, and J. J. Rhyne, Phys. Rev. Lett. **113**, 147203 (2014).
[19] S. Sun, H. Zeng, D. B. Robinson, S. Raoux, P. M. Rice, S. X. Wang, and G. Li, J. Am. Chem. Soc. **126**, 273 (2004).
[20] D. F. Farrell, Y. Ijiri, C. V. Kelly, J. A. Borchers, J. J. Rhyne, Y. Ding, and S. A. Majetich, J. Magn. Magn. Mater. **303**, 318 (2006).
[21] Certain commercial suppliers are identified in this paper to foster understanding. Such identification does not imply recommendation or endorsement by the National Institute of Standards and Technology, nor does it imply that the materials or equipment identified are necessarily the best available for the purpose.
[22] S. R. Kline, J. Appl. Cryst. **39**, 895 (2006).
[23] The uncertainty in the nanoparticle magnetization stems from three repeated atomic absorption measurements to determine iron content in a given quantity of nanoparticles.